RSC Advances

ROYAL SOCIETY OF CHEMISTRY

www.rsc.org/advances

Journal Name

ARTICLE

A Scalable and Facile Synthesis of Alumina/Exfoliated Graphite Composites by Attrition Milling

E. Lee,[a] K. B. Choi,[a] S.-M. Lee, J.-Y. Kim,[a]* J. Y. Jung,[b] S. W. Baik,[b] Y. S. Lim,[c] S. J. Kim,[d] and W. Y. Shim[e]*

Nanostructured carbon-ceramic nanocomposites are becoming important and promising structural materials for plasma-resistant applications because of their electro-conductive and mechanically robust (fracture-, wear-, and plasma-resistant) nature. In this work, we present a facile one-pot synthesis of alumina/exfoliated graphite (EG) composite by attrition milling employing small ceramic beads. The resulting composite shows homogeneous dispersion of exfoliated graphitic nanosheets in the ceramic matrix. The sintered composites exhibit excellent electrical conductivity (>1,000 S/m), fracture toughness (5.6 MPa m$^{0.5}$), and wear resistance, which is enhanced by 7.7 times compared to pure alumina.

Introduction

Due to the outstanding electrical and mechanical properties of carbon nanotubes (CNTs)[1] and graphene sheets,[2] the fabrication of graphene- or CNT-ceramic composites has attracted enormous attentions. Although ceramic composites mechanically reinforced by graphene or CNTs[3,4] have been reported, fabrication of electrically conductive ceramic composites is more promising for electro-ceramic materials. With volume fractions as low as 0.9 vol% for multi-walled carbon nanotubes (MWCNTs)[5] or 3.0 vol %[6] for few-layer graphene (FLG), it is possible to increase the electrical conductivity of ceramic composites by about 14 orders of magnitude.[5-7] This new functionality allows innovative applications of electro-conducting components (cathode, plasma resistant parts, anti-static parts, etc.) in the semiconductor or display manufacturing industries and new possibilities, such as the electro-discharge machining of ceramics.[8]

In general, the high percolation threshold of graphene composites is mainly caused by the limited exfoliation and severe agglomeration of graphene layers. In fact, it is difficult to achieve a high yield of single-layer graphene (SLG) or FLG in ceramic composites without nano-layer agglomeration. It has

been reported that the thickness of graphene layers in ceramic matrices typically varies from 2.5 to 100 nm, and only a low yield of SLG or FLG is achieved,[7,9,10] although SLG and FLG were obtained by sonication or the milling of graphite flakes before mixing with ceramic suspensions.[11]

Since Fan et al. reported exfoliated graphite (EG)/Al$_2$O$_3$ composites synthesized by planetary milling in wet medium,[6] a number of work has been done on the synthesis of graphitic nanosheet (graphene or EG)-ceramic composites by ceramic processing. In fact, it depends on processing condition, whether graphitic nanosheets in ceramic composites are SLG/FLG (1-10 layer; <3.5 nm)[12-15] or EG nanosheets (>10 layer).[6,7,9,10,16-19] The degree of dispersion can be greatly enhanced by colloidal processing, which provides good quality dispersion through modification of surface charges on the ceramic and graphene or EG powder. However, such high-energy-mechanical-milling (HEMM) process as planetary milling, is not easy to be adapted to mass-production because HEMM is small-scale batch process. For mechanical ball-milling with low energy, graphene or EG nanosheets should be prepared by expensive chemical or plasma synthesis prior to ceramic processing. Furthermore, concentration of stable graphitic suspension is often limited to ~1.0 mg/mL, and therefore, such process requires a large volume of graphitic suspension. For example, litres of graphitic suspension (~1 mg/mL) is needed for hundreds gram of composite powder. In this respect, attrition milling using wet medium is an efficient, scalable, environmentally friendly method for EG/ceramic composite synthesis. The schematic of synthesis is shown in Fig. 1a. In wet attrition milling, surface properties of ceramic slurry and graphitic suspension were modified separately, and then mixed to produce composite materials in slurry in a continuous manner, which is advantageous to scalable mass production.(Fig. 1b)

a. Icheon branch, Korea Institute of Ceramic Engineering and Technology, Icheon 467-843, Korea.
b. Maxtech, Daegu 704-920, Korea.
c. Energy and Environmental Division, Korea Institute of Ceramic Engineering and Technology, Jinju-si 660-031, Korea.
d. Department of Chemistry, Division of Energy Systems Research, Ajou University, Suwon 443-749,Korea.
e. Department of Materials Engineering, Yonsei University, Seoul 120-749, Korea.

RSC Advances Accepted Manuscript

In this work, we attempted to synthesize an alumina/exfoliated graphite (EG) composite by a scalable attrition milling method using expanded graphite (Exp-G) as a raw material. This technique provides a facile one-pot synthetic method to produce an alumina/EG composite. The EG with the nature of an unoxidized graphitic network unlike conventional graphene oxide was successfully exfoliated into nanosheets, which were uniformly dispersed in the ceramic matrix with the aid of non-covalent functionalization via π-π interaction. The electrical conductivity of the alumina/EG composites shows metal-insulator transition with a percolation threshold of ~5.2 vol% with an increase of ~11 orders of magnitude. The fracture toughness and wear resistance of the composites were found to increase by ~75 % and 7.7 times, respectively, compared to those of pure alumina.
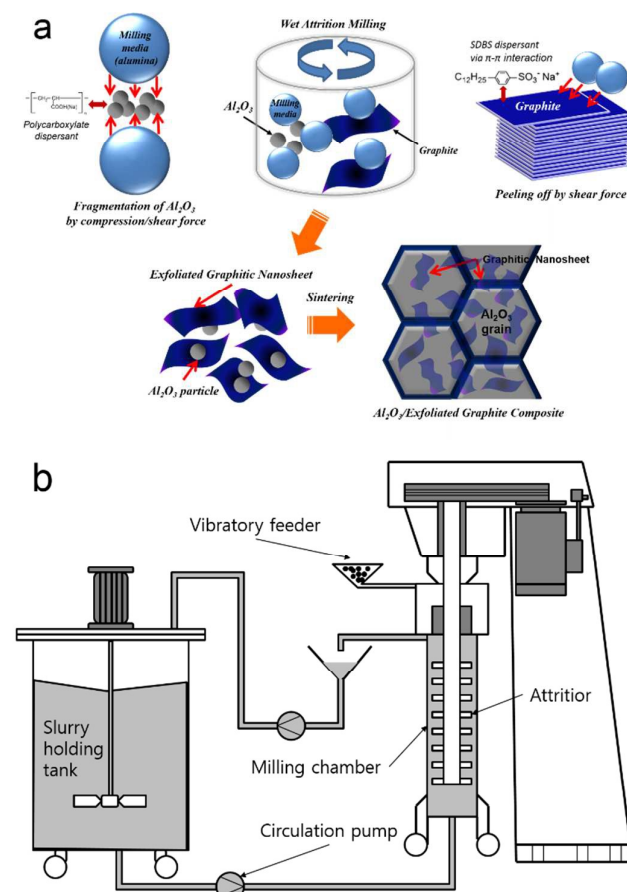
Fig. 1. (a) Schematic of the synthesis of Al_2O_3/exfoliated graphite(EG) composite by attrition milling in wet medium. Small ceramic ball size (~2mm) creates a higher probability of ball-to-ball or ball-to-vial impact and shearing on the crystals, compared to conventional planetary milling. Gentle shear force due to the use of lighter weighted beads minimizes damages of nanosheets. Al_2O_3 and EG were readily dispersed by polycarboxylate and sodium dodecylbenzenesulfonate, respectively, and mixed/aged to produce Al_2O_3/EG composite slurry. (b) Schematic of attrition milling machine using wet medium. Scalable and continuous synthesis is enabled by circulation of slurry in holding tank and milling chamber.

Experimental

Alumina/EG Composite Synthesis. First, alumina powder (>99 %, 160SG, Showa Denko) was added to distilled water (60 wt%) with polyvinyl alcohol (PVA-205, Kuraray, 1.5 wt%) and polycarboxylate ammonium (Cerasperse 5468CF, San Nopco) as a binder and a dispersant, respectively. Then, expanded graphite (Exp-G) or graphite oxide (GO4401, IDT International) powder was added to the aqueous slurry with concentrations of 1.0, 2.5, 3.0, 5.0 wt%. The Exp-G was obtained by heating expandable graphite (Grafguard 160-50N, Graftech, USA) at 800℃ for 1 h, which was expanded by 200 times. Dispersants for nanocarbons, polycarboxylate ammonium (Cerasperse 5468CF) and sodium dodecylbenzenesulfonate (SDBS, Sigma Aldrich) for GO and EG, respectively, were added by 1.0 wt% of alumina. To obtain a homogeneous suspension, the aqueous slurry was ball milled by attrition mill (Nanoset mill NS-005, DNTEK, Korea) using YTZ balls (φ=2.0 mm) as a medium for 3 h with a speed of 3000 rpm. Ball to powder weight raio was 4:1. Ball milling was performed in distilled water-based wet condition, where temperature is controlled by cooling water. The milled slurry was dried using a spray dryer (HCSY-01, Hwachang Eng., Korea). The drying conditions were the following: hot air temp.: 180℃, exhaust air temp.: 80℃, disc rotation speed: 8500 rpm, slurry feeding rate: 0.3L/min). The dried powder had a uniform granule-like shape with high flowability. (water content: 0.5 wt%) The additives of dispersant or binder were removed by calcination at 600℃ for 2 h in a vacuum furnace with Ar gas flow. After de-binding, the mass loss was found to be ~2 wt%, which was consistent with additive content (2 wt%). The calcined powder was sintered by hot press (VHP-400T, Samyang Ceratech, Korea) in an N_2 flowing atmosphere. The temperature was raised at a rate of 20~25℃/min and maintained at 1500 ℃ for 1 h with a pressure of 20MPa.

Electrical conductivity Measurement. The surface resistance was measured by a resistance meter (Trek Resistance meter 152-1) using the two-probe method according to STM11.11 (Surface resistance measurements of static Dissipative Planar Materials) of ANSI/ESD association standards. The volume resistivity was measured by a resistance meter (Trek Resistance meter 152-1) using the guarded electrode method according to IEC 61340-2 of ANSI/ESD association standards.

Mechanical Property Measurement. The hardness of the sintered speciemens was measured by a Vickers Microhardness Tester (MXD-CX3E, Matsuzawa, Japan). A load of 10 kgf was applied for 10 s. Hardness was measured 5 times and calculated according to the following equation: HV = 1.8544 P/a^2. (P: Applied load, a: diameter of indentation) The fracture toughness was measured by the indentation fracture (IF) method. The micro-hardness testing technique was used to induce radial cracking from the corners of the indentation. A mirror-finished surface was indented by a Vickers hardness

machine. The indentation loads were 98 N. The fracture toughness was calculated by the Antis equation.

$$K_{IC} = 0.16 \left(\frac{E}{H}\right)^{1/2} \frac{P}{C_0^{3/2}}$$

K_{IC}: Fracture toughness, E: Young's modulus, H: Hardness, C_0: Crack length, P: Applied load

Tribological Property Measurement. Tribological measurements were performed at room temperature using a multi-purpose tribometer (MPW 110, Neoplus inc.) with a ball on disk contact geometry according to KS L 1606 (Determination of friction and wear characteristics of monolithic ceramics by ballon-disc method). The surfaces were carefully prepared by polishing down to a surface roughness below 0.04 μm. As a counterpart, tungsten carbide balls of 9.5 mm diameter was used. The normal load during the tribotests was set to 50 and 100 N load and a wear track of 11.5 mm radius were used in each flat. The sliding speeds for the wear rate and friction coefficient measurements were 10 cm/s and 12.5 cm/s, respectively. The total wear cycles were 27,700 (2,000 m) and 1,250 (90 m), respectively. Masses of specimens were measured before and after tests, which were divided by density to obtain the wear volume. The wear volume was divided by load and distances to get wear rate.

Results and discussion

Synthesis of Alumina/EG Composite by Mechanical Milling. Ball milling has been reported to synthesize graphitic flakes,[20-22] however, this method is not successful to obtain graphene with thicknesses less than 10 nm. Recently, ball milling techniques employing higher mechanical energy such as planetary milling using a medium (DMF, CO_2, melamine, salt)[23–26] and stirred media milling using smaller media[27,28] has been found to be effective to produce graphenes. The high mechanical energy of planetary milling is favourable for the exfoliation of graphite, while its drawbacks are long processing time (several tens of hours), a post-dispersing step using sonication due to low yield, and the lack of scalability of planetary milling (batch-type process). On the other hand, stirred media milling techniques such as attrition milling provides remarkably enhanced delamination yields and scalability (continuous process) of graphite exfoliation.

In this work, we adopted a attrition milling technique that utilizes small beads (~2 mm in diameter) as a milling media to allow the exfoliation of expanded graphite (Exp-G) and pulverization/dispersion of alumina powder simultaneously. To retain the excellent electrical and mechanical properties of graphitic flakes, Exp-G, which did not undergo a severe chemical oxidation process, was used as a raw materials. To disperse Exp-G with a hydrophobic nature in an aqueous alumina slurry, an anionic surfactant, sodium dodecylbenzenesulfonate (SDBS), which is able to achieve noncovalent functionalization of the EG surface, was used.[29,30] The exfoliation of Exp-G and pulverization of a ceramic (alumina) material can be achieved by one-pot facile synthesis

in a continuous fashion. The attrition milling process can be operated in a continuous fashion, which is highly advantageous for mass production. Furthermore, the process is eco-friendly because no non-aqueous medium was involved in synthetic process.
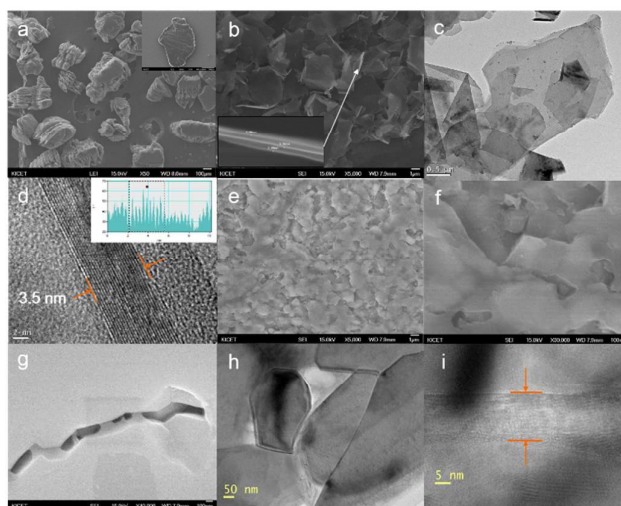
Fig. 2. SEM images of (a) thermally expanded graphite (Exp-G). Inset shows expandable graphite before thermal treatment (b) SEM images for exfoliated graphites by attrition milling. (c) TEM images for exfoliated graphites. (d) High-resolution TEM (HRTEM) images of exfoliated graphite nanosheets, which shows layer thickness of 3.5 nm. (e) SEM images of the fracture surface for 9.4 vol% EG/Al_2O_3 composite. (f) The enlarged image of (e), showing a thin layer of EG present between grains. (g) The embedded EG in grains that is exposed in the micro-crack of the EG/Al_2O_3 composite, which was generated by Vickers indentation. (h) TEM image of 9.4 vol% EG/Al_2O_3 composite (i) high-resolution TEM image of the EG layers in composites.

Dispersion of Al_2O_3/EG composite. In the present synthesis of composites, expandable graphite (inset of Fig. 2a) was used as a raw material. Exp-G (Fig. 2a) was obtained by heating expandable graphite at 800℃ for 1 h, which was expanded by ~200 times. As shown in Fig. 2b-d, EG nanosheets can be readily obtained by attrition milling or ultrasonication of aqueous Exp-G suspension with SDBS surfactant. Fig. 2ef shows EG nanosheets homogeneously dispersed in sintered alumina matrix. Fig. 2g shows embedded EG in alumina matrix, which is exposed in crack propagation pathway made by Vickers indentation. Fig. 2hi shows thin EG layers (THK: 10~20 nm) in alumina matrix.

In order to obtain homogeneous mixture of aqueous alumina and EG nanosheet suspension, the dispersion stability of EG suspension was studied first. As shown in Fig. 3a, EG nanosheets with hydrophobic nature can be dispersed well in DMF (left), not in water (middle). Dispersion of EG nanosheets in water was enabled by surface modification by SDBS as shown in Fig. 3a (right). This means that stable mixture of aqueous alumina particles with hydrophobic EG needs surface modification of EG nanosheets. The dispersion stability of the alumina/EG slurry was compared with that of alumina/graphite oxide (GO) slurry.(Fig. 3b) GO was produced by modified Hummer's method using graphite, which has diverse functional groups (-COOH, -C=O, -OH) that can be

ARTICLE   Journal Name

converted into other groups or covalent bonding to nanoparticles or polymers. To evaluate dispersion stability, two kinds of dispersant were applied to the alumina/EG and alumina/GO slurries. Anionic surfactants, polycarboxyl ammonium (PCA) and SDBS, were used. The former has been effective in the dispersion of metal oxide, and the latter is reported to be effective in dispersing nanocarbons such as CNTs and graphene due to strong noncovalent π-π interaction (Fig. 3a).[29,30] As shown in Fig. 3b, SDBS is not a suitable dispersant for alumina/GO slurry (①) since it has relatively low polarity for dispersing alumina particles and GO. PCA is an excellent dispersant for alumina and GO, but it is not good for EG. Therefore, the alumina/GO slurry using PCA (②) shows good stability, while, in the alumina/EG slurry using PCA (③), the EG tends to precipitate and segregate from alumina particles. Therefore, because of the stronger ability of SDBS to disperse carbon species with graphitic network, we used SDBS and PCA separately as dispersants for the EG suspension and alumina, respectively. As shown in Fig. 3b, the alumina/EG slurry (④), which was dispersed by SDBS/PCA, showed better dispersion stability after 24 h than the slurries treated with a single dispersant. The EG suspension, dispersed by attrition milling using SDBS as a dispersant, was mixed with alumina slurry, which was dispersed using PCA, and then the mixture was mechanically milled by attrition milling. As shown in Fig. 3c and 3d, sintered specimen from slurry dispersed by SDBS/PCA(④) shows better dispersion of graphitic sheets in the alumina matrix, compared to that by PCA(③).
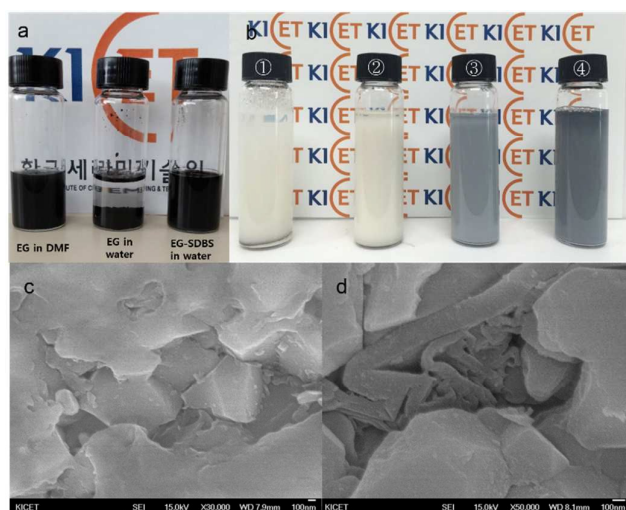
Fig. 3. (a) exfoliated graphite (EG) dispersions in DMF, in water, and aqueous EG dispersion functionalized by SDBS (from left to right). (b) ① alumina/GO slurry (SDBS dispersant), ② alumina/GO slurry (PCA dispersant), ③ alumina/EG slurry (PCA dispersant), ④ alumina/EG slurry (SDBS/PCA mixed dispersant). The slurries were placed for 24 h after milling process. (c) Fracture surface of 9.4 vol% EG/Al₂O₃ composite from suspension dispersed by SDBS/PCA(④). (d) Fracture surface of alumina/EG composite from suspension dispersed by PCA(③). Thick unexfoliated graphite and agglomerated graphitic sheets are observed in ③.

Electrical property of Alumina/EG composites. Based on the comparative study of the dispersion of the present slurries, alumina and EG were mechanically dispersed separately by

attrition milling using dispersants of PCA and SDBS, respectively, and then they were mixed and milled by attrition milling again to obtain a homogeneous and well dispersed suspension of their mixture. Next, the resulting slurry was dried by a spray dryer and were sintered by a hot press at 1500 ℃ for 1 h with a pressure of 20 MPa.

The electrical resistivity of the composites at room temperature are shown in Table 1. According to the resistivity versus EG concentration, below 4.7 vol% of EG, the resistivity decreases slowly with increasing EG concentration, while the resistivity abruptly decreases at 5.7 vol% of EG (Fig. 4). This phenomena can be explained by metal-insulator (MI) transition by percolation theory.[31,32] In the present composites, the percolation threshold is 2.5~3.0 wt% (4.7~5.7 vol%) and MI transition occurs in this region, which results in enhanced electrical conduction by several orders of magnitude. The threshold value is much larger than that of alumina/FLG (few-layered graphene) composites (~0.38 vol%),[12] while it is similar to the percolation threshold of ~3.0 vol% found in alumina/FLG composites synthesized by planetary milling. This is probably due to the larger thickness of the dispersed EG nanosheets in comparison to FLG. The thickness of the EG nanosheets is assumed to similar to that of alumina/FLG by planetary milling. According to HRTEM analysis (Fig. 2i), the thickness of the embedded EG layer is shown to be 10~20 nm.

Table 1. Electrical resisitivity of alumina/EG composites

Compd	Al₂O₃	1.9 vol% EG/Al₂O₃	4.7 vol% EG/Al₂O₃	5.7 vol% EG/Al₂O₃	9.4 vol% EG/Al₂O₃
Resistivity (Ω cm)	>5.0E15	1.0E14	1.0E13	8.75E5	1.04E3

According to percolation theory, the electrical conductivity of the composite material containing metallic filler (M) in a dielectric matrix (D) is given by the power law as follows.[33]

$$\langle \sigma \rangle = \sigma_M (f - f_c)^t \qquad f > f_c \qquad (1)$$

$$\langle \sigma \rangle = \sigma_D (f_c - f)^{-q} \qquad f < f_c \qquad (2)$$

σ_D : conductivity of dielectric material, σ_M : conductivity of metallic filler, f : volume fraction of dielectric and conducting filler, t=critical exponent before percolation threshold, q= critical exponent after percolation threshold

Plotting Log(conductivity) vs Log(F-Fc) linearly, we can calculate the σ(D), σ(M), t, and q values. Fitted values according to equations (1) and (2) are quite consistent with the experimental values.(Fig. 4) These parameters are given in Table 2. The fitted t value of 2.89 in the present system is rather larger than the reported values for mullite-molybdenum cermet (1.6)[34] and alumina-FLG composite (1.84).[12] In percolation theory based on a discrete lattice-percolation network, the t values are 1.3 and 2.0 in 2D- and 3D-systems, respectively, while much larger t values (2< t <3) have also been found experimentally and theoretically in continuum percolation networks.[28-30,42-47] Several groups have experimentally measured conductivity critical exponents close to or greater than 3.0 in similar types of polymer-conductor[38-40] and ceramic-conductor composites.[41,44] These experimental

discrepancy has been interpreted as a fundamental difference between continuum percolation and lattice percolation.[42] Such behaviour was theoretically explained as a result of anomalous diverging distribution of resistances between the conductive elements,[43] or a quantum tunnelling model of conduction between the conductive elements,[40] or "Swiss-cheese model" where spherical voids are introduced in a continuous conductor.[37]

Table 2. Fitted parameters by eqns. (1) and (2) from electrical resisitivity of the composites

σ_D (S/cm)	σ_M (S/cm)	f_c	q	t
2.0E-16	10	0.0525	1.2532	2.8923
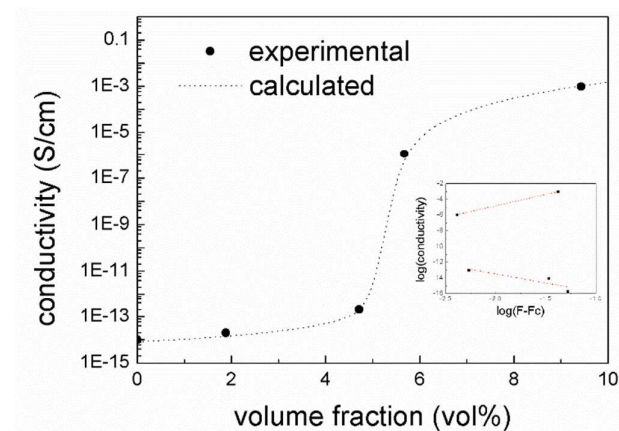
Fig. 4. Electrical conductivity of alumina/EG composites as a function of EG volume fraction. Experimental data were fitted by calculated curve according to Eqn.s (1) and (2).
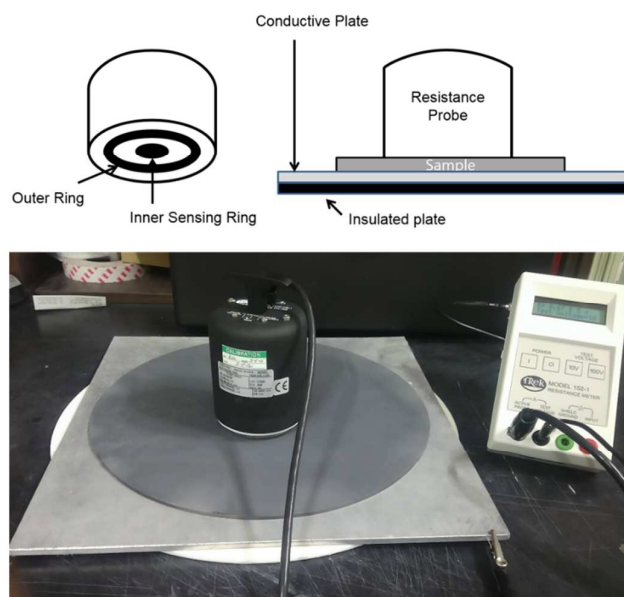
Fig. 5. Electrical conductivity measurements of sintered alumina/EG composite.

Mechanical Properties of Alumina/EG Composite. The fracture toughness of the alumina/EG composite was enhanced upon the embedding of EG in the alumina matrix. The K_{IC} value of the 1.9 vol% EG/Al_2O_3 composite (5.62 MPa $m^{0.5}$) was increased by ~75% compared to that of pure alumina (3.2 MPa $m^{0.5}$). The average grain sizes for pure alumina and the EG composite were 1.6~2.0 and 1.5~1.8 μm, respectively, which indicates that the increased toughness is not consistently explained by the Hall-Petch relationship. The grain size was calculated by intercept method using SEM images of EG/Al_2O_3 composites. (Supporting information) Fig. 2g shows abundant bridges behind the crack tip, which were produced by Vickers indentation. Even though the observed bridging might not be due to single-layer graphene, it shows clearly that EG nanosheets contribute to bridging. Such a bridging mechanism has been widely reported in ceramic composites containing a few vol% of whiskers,[45] fibers,[46] and graphene.[13,47]

The EG embedding in the alumina matrix was found to significantly enhance not only the toughness but also the wear resistance of the composites due to its tribological effect. In the regime under a high normal load (load: 100 N, sliding speed: 100 mm/s, wear distance: 90 m), the use of EG as an additive (5.7 vol%) in the matrix resulted in a marked reduction of the wear rate from 2.1×10^{-4} mm^3/N·m to 2.7×10^{-5} mm^3/N·m by a factor of ~7.7. It appears that reduced friction due to EG embedding could significantly improve wear resistance. The friction coefficients (COF) decreased from 0.637 (pure alumina) to 0.496 for the 5.7 vol% EG/Al_2O_3 composite. In the condition of a lower normal load with higher speed (load: 50 N, sliding speed: 125 mm/s, wear distance: 2,000 m), no discernible mass loss or measurable track was observed even after prolonged duration cycles, which means that the dominant mechanism is sliding wear rather than abrasion wear. Remarkably improved wear resistance of the composites appear to be related to less grain pull-out during wear process and higher fracture toughness. According to previous study, the wear process of alumina consists of two steps: deformation dominated- and grain pull-out dominated-wear.[48] Reduced wear track in the present samples show that the EG addition to the alumina matrix reduced grain pull-out. This reduced pull-out might be due to less tangential force applied to alumina grains, which can be attributed to reduced friction and EG addition.[47]

However, higher loading of EG up to 9.4 vol% in the alumina matrix resulted in an increased wear rate of 8.1×10^{-5} mm^3/N·m, compared to that of the EG (5.7 vol%) composite. This result shows that improvements in the wear resistance of the composites may be also related to their fracture toughness because composites with excessive EG loadings should have lower fracture toughness. Although the reduced friction of the alumina/EG composite mainly contributes to the reduction of the wear rate, it appears that enhanced fracture toughness, also enhances wear resistance.[47,48]

Conclusions

In this work, a facile, scalable, one-pot synthesis of ceramic/graphitic nanosheet composites by low-energy ball milling was demonstrated. The use of polycarboxylate and SDBS as dispersants for alumina and graphitic nanosheets, respectively, effectively produced well-dispersed slurry of alumina/graphitic nanosheet composite. The sintered composites exhibit excellent electrical conductivity (>1,000 S/m), fracture toughness (5.6 MPa m$^{0.5}$), and wear resistance, enhanced by 7.7 times compared to pure alumina. This approach provides a facile route to electro-conductive and mechanically robust ceramic-graphite composite with innovative applications of electro-conducting components (cathode, plasma resistant parts, anti-static parts, etc.) in the semiconductor or display manufacturing industries.

Acknowledgements

Notes and references

‡ Footnotes relating to the main text should appear here. These might include comments relevant to but not central to the matter under discussion, limited experimental and spectral data, and crystallographic data.
§
§§
etc.

1   M. S. Dresselhaus, G. Dresselhaus, J. C. Charlier and E. Hernandez, *Philos. Trans. Roy. Soc. Lond. A* 2004, **362**, 2065.
2   A. K. Geim and K. S. Novoselov. *Nat. Mater.*, 2007, **6**, 183.
3   G. D. Zhan, J. D. Kuntz, J. Wan and A. K. Mukherjee, *Nat. Mater.*, 2002, **2**, 38.
4   X. Wang, N. P. Padture and H. Tanaka, *Nat. Mater.*, 2004, **3**, 539.
5   J. Gonzalez-Julian, Y. Iglesias, A. C. Caballero, M. Belmonte, L. Garzo´n, C. Ocal, P. Miranzo, M. I. Osendi, *Compo. Sci. Tech.* 2011, **71**, 60.
6   Y. Fan, L. Wang, J. Li, S. Sun, F. Chen, L. Chen, W. Jiang, *Carbon*, 2010, **48**, 1743.
7   (a) C. Ramirez, F. Figueiredo, P. Miranzo, P. Poza, M. I. Osendi, *Carbon*, 2012, **50**, 3607. (b) C. Ramirez, L. Garzon, P. Miranzo, M. I. Osendi, and C. Ocal, Carbon, 2011, 49, 3873.
8   O. Malek, J. Gonzalez-Julian, J. Vleugels, W. Vanderauwer, B. Lauwers, M. Belmonte, *Mater. Today*, 2011, **14**, 496.
9   J. Dusza, J. Morgiel, A. Duszova, L. Kvetkova, M. Nosko, P. Kun, C. Balazsi, *J. Eur. Ceram. Soc.*, 2012, **32**, 3389.
10 T. He, J. Li, L. Wang, J. Zhu, W. Jiang, *Mater. Trans.* 2009, **50**, 749.
11 M. V. Antisari, A. Montone, N. Jovic, E. Piscopiello, C. Alvania and L. Pilloni, *Scr. Mater.*, 2006, **55**, 1047.
12 Y. Fan, W. Jiang and A. Kawasaki, *Adv. Func. Mater.*, 2012, **22**, 3882.
13 L.S. Walker, V. R. Marotto, M. A. Rafiee, N. Koratkar and E. L. Corral, *ACS Nano*, 2011, **5**, 3182.
14 H. Porwal, P. Tatarko, S. Grasso, J. Khaliq, I. Dlouhy, M. J. Reece, *Carbon*, 2013, **64**, 359.
15 C. Ramirez, S. M. Vega-Diaz, A. Morelos-Gomez, F. M. Figueiredo, M. Terrones, M. I. Osendi, M. Belmonte, P. Miranzo, Carbon, 2013, 57,425.
16 M. Belmonte, C. Ramirez, J. Gonzalez-Julian, J. Schneider, P. Miranzo, M. I. Osendi, Carbon, 2013, 61, 431.
17 G. B. Yadhukulakrishnan, S. Karumuri, A. Rahman, R. P. Singh, A. K. Kalkan, S. P.Harimkar, Ceram. Intern. 2013, 39, 6637.
18 A. Nieto, L. Huang, Y.-H. Han, J. M. Schoenung, Ceram. Int., 2015, 41, 5926.
19 K. Wang, Y. Wang, Z. Fan, J. Yan, T. Wei, Mater. Res. Bull., 2011, 46, 315.
20 M. Antisari, A. Montone, N. Jovic, E. Piscopiello, C. Alvani and L. Pilloni, *Scr. Mater.*, 2006, **55**, 1047.
21 A. Milev, M. Wilson, G. S. K. Kannangara and N. Tran, *Mater. Chem. Phys.,* 2008, **111**, 346.
22 R. Janot and D. Guerard, *Carbon*, 2002, **40**, 2887.
23 W. Zhao, M. Fang, F. Wu, H. Wu, L. Wang and G. Chen, *J. Mater. Chem.,* 2010, **20**, 5817.
24 I. Y. Jeon, Y. R. Shin, G. J. Sohn, H. J. Choi, S. Y. Bae, J. Mahmood, S. M. Jung, J. M. Seo, M. J. Kim, D. Wook Chang, L. Dai and J. B. Baek, *Proc. Natl. Acad. Sci. U. S. A.*, 2012, **109**, 5588.
25 V. Leon, A. M. Rodriguez, P. Prieto, M. Prato and E. Vazquez, *ACS Nano*, 2014, **8**, 563.
26 Y. Lv, L. Yu, C. Jiang, S. Chen and Z. Nie, *RSC Adv.*, 2014, **4**, 13350.
27 C. Damm, T. J. Nacken and W. Peukert, *Carbon*, 2015, **81**, 284.
28 C. Knieke, A. Berger, M. Voigt, R. N. K. Taylor, J. Rohrl and W. Peukert, *Carbon*, 2010, **48**, 3196.
29 M. F. Islam, E. Rojas, D. M. Bergey, A. T. Johnson and A. G. Yodh, *Nano Lett.*, 2003, **3**, 269.
30 D. Parviz, S. Das, H. S. T. Ahmed, F. Irin, S. Bhattacharia and M. J. Green, *ACS Nano*, 2012, **6**, 8857.
31 S. Kirkpatrick, *Rev. Mod. Phys.*, 1973, **45**, 574.
32 D. Stauffer, *Phys. Rep.*, 1979, **54**, 3.
33 A. L. Efros and B. I. Shklovskii, *Phys. Stat. Sol. (B)*, 1976, **76**, 475.
34 C. Pecharroman, J. S. Moya, *Adv. Mater.*, 2000, **12**, 294.
35 B. I. Halperin, S. Feng and P. N. Sen, *Phys. Rev. Lett.*, 1985, **54**, 2391.
36 M. B. Heaney, *Phys. Rev. B: Cond. Mat.*, 1995, **52**, 12477.
37 S. Feng, B. I. Halperin and P. N. Sen, *Phys. Rev. B: Cond. Mat.*, 1987, **35**, 197.
38 A. Quivy, R. Deltour, A. G. M. Jansen, P. Wyder, Phys. Rev. B, 1989, 39, 1026.
39 F. Carmona, A. El Amarti, Phys. Rev. B, 1987, 35, 3284.
40 I. Balberg, Phys. Rev. Lett., 1987, 59, 1305.
41 S. Lee, Y. Song, T. W. Noh, X.-D. Chen, J. R. Gains, Phys. Rev. B, 1986, 34, 6719.
42 I. Balberg, Philos. Mag. B, 1987, 56, 99.
43 P. M. Kogut and J. P. Straley, J. Phys. C 1979, 12, 2151.
44 K. Waku, H. Hayashi, A. Kishimoto, J. Amer. Ceram. Soc., 2008, 91, 4168.
45 P. F. Becher, C.-H. Hsueh, P. Angelini and T. N. Tiegs, *J. Am. Ceram. Soc.*, 1988, **71**, 1050.
46 K. Niihara, K. *J. Ceram. Soc. Jpn.*, *1991*, **99**, 974.
47 H. J. Kim, S.-M. Lee, Y.-S. Oh, Y.-H. Yang, Y. S. Lim, D. H. Yoon, C. Lee, J.-Y. Kim and R. S. Ruoff, Sci. Rep. 2014, **4**, 5176.
48 S. J.Cho, B. J. Hockey, B. R. Lawn and S. J. Bennison, *J. Am. Ceram. Soc.*, 1989, **72**, 1249.